CMAF PrePrint Pre-2011-003
http://cmaf.ptmat.fc.ul.pt/preprints.html

Damage identification in a concrete dam by fitting measured modal parameters

Sérgio Oliveira, Anca-Maria Toader, Paulo Vieira

S. Oliveira
Núcleo de Modelação Matemática e Física, Departamento de Barragens de Betão, LNEC, Av. do Brasil, 101, 1700-066 Lisbon, Portugal
*(*soliveira@lnec.pt*)*

A.M. Toader, P. Vieira
CMAF, Universidade de Lisboa, Av. Prof. Gama Pinto, 2, 1649-003, Lisbon, Portugal
*(*amtan@ptmat.fc.ul.pt, pvieira@ptmat.fc.ul.pt*)*

Abstract. Given accurate measurements of the first modal parameters, namely the natural frequencies and the modes of vibration (the eigenfrequencies and the eigenvectors) of a solid body with linear elastic behavior, the material parameters that characterize the elasticity tensor of a model of the body are numerically identified through an inverse problem. Appropriate functionals are defined, whose minimum points correspond to the unknown material parameters. The main tools used to obtain these minimum points are parametric optimization, the derivative of the eigenvalues and eigenvectors with respect to the material parameters, the adjoint method, and gradient methods for the minimization of the functionals. An application, considering a cracked dam in which is assumed the presence of transversely isotropic material in the cracked zone, is presented. The material parameters concerning the transversely isotropic material are obtained by minimizing the distance between the modal parameters of a numerical model of the dam and the observed modal parameters (physically measured in the dam).

Keywords: Inverse problem, Material parameter identification, Derivatives of eigenvalues and eigenvectors, Adjoint problem.

1. Introduction

When using numerical models to simulate the behavior of dams, it is of utmost importance to choose appropriate values for the elastic material parameters of the model in order to attain coherent results with experimental physical measurements. Therefore, the determination of the material parameters of solids is a problem in engineering to which several methods have been devised over the last years (Mota Soares, 1993), (Pagnotta, 2008). With the increase of computing power in recent years, the mixed numerical/experimental methods gained relevance. Briefly, these methods consist in the formulation of an inverse problem defined from experimental data measured in advance in the

considered body, as the natural frequencies or modes of vibration. An appropriate linear elastic model of the body is chosen, and a functional that depends on the material parameters of the model is then defined. This functional measures in some way the error between the experimental data and the corresponding data from the model. The values that minimize this functional correspond to material parameters such that the elastic model fits best the observed data and consequently should be appropriate to describe the elastic properties of the body. This approach is close to the field of Free Material Optimization, as presented in (Bendsoe, 1995).

The experimental data used are the first natural frequencies and vibration modes of the Cabril dam, located in Portugal (CNPGB, 1992). These frequencies and vibration modes are being continuously identified from data obtained with vibration measurement equipment installed on the dam (Oliveira, 2002), (Oliveira, 2011). Accordingly, a chosen objective functional can be defined as a least square type distance of the natural frequencies,

$$s \mapsto J_1(s) = \sum_{i=1}^{n} |\omega_i(s) - \tilde{\omega}_i|^\alpha, \tag{1}$$

or, considering both natural frequencies and vibration modes, another proposed objective functional will be

$$s \mapsto J_2(s) = \sum_{i=1}^{n} |\omega_i(s) - \tilde{\omega}_i|^\alpha + \|u_i(s) - \tilde{u}_i\|^\alpha_{L^2_\rho}\,. \tag{2}$$

In the above, n is the number of natural frequencies and vibration modes taken into account, $\tilde{\omega}_i$ is the i-th natural frequency that was experimentally measured in the dam, and $\omega_i(s)$ is the corresponding natural frequency of the linear elastic model. In the same way, $\tilde{u}_i$ is the i-th measured vibration mode and $u_i(s)$ is the corresponding vibration mode of the elastic model. The power $\alpha > 0$ should be adjusted in a convenient manner (generally $\alpha = 2$). The norm $\|\cdot\|_{L^2_\rho}$ on the space $L^2(\Omega)^3$ is induced by the following inner product associated to the function representing the specific mass $\rho \in L^\infty(\Omega)$ ($\rho(x) \geq \rho_0 > 0$ almost everywhere in Ω):

$$(u, v) \mapsto \int_\Omega \rho u \cdot v \, dx\,.$$

The material parameters are denoted by s, which in this case can be represented as an m-tuple in $\mathbb{R}^m$ (that is, the model has m material parameters $s_1, \ldots, s_m$). The natural frequencies $\omega_i(s)$ of the model

are calculated as $\frac{\sqrt{\lambda_i}}{2\pi}$, where λ_i are the eigenvalues of the eigenvalue problem associated to the system of equations of linearized elasticity:

$$\begin{cases} -div(\mathbf{C}\epsilon(u)) &= \lambda\rho u \ \text{ in } \Omega, \\ u &= 0 \ \text{ on } \Gamma_D, \\ \mathbf{C}\epsilon(u)\cdot n &= 0 \ \text{ on } \Gamma_N. \end{cases} \tag{3}$$

The vibration modes u_i are the eigenvectors of problem (3). In this problem we assume that the body occupies the domain $\Omega \subset \mathbb{R}^3$ and the boundary $\partial\Omega$ is split in two disjoint parts: the part Γ_D, where the Dirichlet condition is applied (where the dam is fixed), and the part Γ_N, where the Neumann condition is applied (the case of an empty reservoir is modeled, therefore the dam is free of surface loads). The symbol $\mathbf{C} = \mathbf{C}(s)$ denotes the fourth-order elasticity tensor and depends on the material parameters s chosen for the considered model, so the solutions $(\lambda_i(s), u_i(s))_{i\geq 1}$ of the eigenvalue problem (3) depend on s as well. The symbol ϵ denotes the strain tensor and ρ the specific mass (density) of the material, which may vary in different parts of the domain. The eigenvalue problem (3) arises from the equations of linearized elasticity considering zero damping and zero external forces:

$$\begin{cases} \rho\dfrac{\partial^2\mathbf{u}}{\partial t^2} - div_x(\mathbf{C}\epsilon(\mathbf{u})) &= 0 \quad \text{in } \ \mathbb{R}^+\times\Omega, \\ \mathbf{u} &= 0 \quad \text{on } \mathbb{R}^+\times\Gamma_D, \\ \mathbf{C}\epsilon(\mathbf{u})\cdot n &= 0 \quad \text{on } \mathbb{R}^+\times\Gamma_N, \\ \mathbf{u}(0,x) &= u_0 \ \text{ on } \Omega, \\ \dfrac{\partial\mathbf{u}}{\partial t}(0,x) &= v_0 \ \text{ on } \Omega. \end{cases} \tag{4}$$

Searching for solutions of the form $\mathbf{u}(t,x) = \phi(t)u(x)$ in system (4), one concludes that the function $u = u(x)$ must satisfy the eigenvalue problem (3). The solutions of (4) in the indicated form represent oscillatory motions, with $u(x)$ representing the modes of vibration of the body.

The minimization of the objective functionals J_1 and J_2 defined above is accomplished with gradient-based methods, namely the BFGS method with an appropriate line-search algorithm. For that purpose, the analytic expression of their derivatives with respect to a generic parameter s have been derived. These expressions, (10) and (13), depend on the natural frequencies $\omega_i(s)$, the modes of vibration $u_i(s)$, and the adjoint states p_i. To obtain the solutions of the eigenvalue problem (3) a finite element discretization of the dam is used and Lanczos method for eigenvalues is applied. The adjoint states are obtained as solutions of n elliptic problems (12), which are solved using the finite element

method. All the minimization algorithm was implemented in a C++ code with the aid of open-source libraries for scientific computation.

2. Derivatives of the natural frequencies and modes of vibration

In order to obtain the derivatives of the natural frequencies and modes of vibration, the variational formulation of the eigenvalue problem (3) is used. For a fixed parameter s, the (weak) solutions $(\lambda(s),\, u(s))$ of the eigenvalue problem (3) are the solutions of the following variational problem:

$$\left\{ \begin{array}{c} \text{find} \;\; \lambda(s) \in \mathbb{R} \;\; \text{and} \;\; u(s) \in V \text{ such that} \\ \displaystyle\int_\Omega \mathbf{C}(s)\, \epsilon(u(s)) \cdot \epsilon(v)\, dx = \lambda \int_\Omega \rho u(s) \cdot v\, dx, \;\; \forall v \in V, \end{array} \right. \tag{5}$$

where the space V of test functions is defined as

$$V = \{v \in H^1(\Omega)^3 : v_{|\Gamma_D} = 0\}.$$

A classical result states the existence of a countably infinite set of solutions of problem (5), with the eigenvalues $(\lambda_i)_{i\geq 1}$ forming an increasing sequence of real numbers, the eigenvectors $(u_i)_{i\geq 1}$ forming an hilbertian basis of L^2_ρ, and such that the pair (λ_i, u_i) verifies problem (3) in the almost everywhere sense, for all $i \geq 1$ (see chapter XII of (Dautray, 1985) for the details).

For simplicity of the exposition, we will assume that the material model in consideration for the body Ω has only one material parameter $s \in \mathbb{R}$. However the following results hold in the vectorial case that is analysed in the numerical simulations.

THEOREM 1. *Provided differentiability properties of the elasticity tensor $\mathbf{C} = \mathbf{C}(s)$ with respect to a general material parameter s and assuming that the eigenvalues of problem (3) are simple, then the eigenvalues and the eigenvectors are differentiable with respect to s.*

The derivative of the eigenvalue $\lambda_i = \lambda_i(s)$ is

$$\frac{d\lambda_i}{ds} = \int_\Omega \frac{d\mathbf{C}}{ds}(s)\epsilon(u_i) \cdot \epsilon(u_i)\, dx, \tag{6}$$

where the corresponding eigenvector u_i is normalized in L^2_ρ: $\|u_i\|_{L^2_\rho} = 1$.

The derivative $\dfrac{du_i}{ds}$ *of the eigenvector* $u_i = u_i(s)$ *is the solution of the problem below:*

$$\left\{\begin{array}{c} \textit{find} \quad \dfrac{du_i}{ds} \in < u_i >^{\perp} \ \textit{such that} \\ \\ \displaystyle\int_\Omega \mathbf{C}(s)\epsilon(\frac{du_i}{ds}) \cdot \epsilon(v)\, dx - \lambda_i \int_\Omega \rho \frac{du_i}{ds} \cdot v\, dx = \\ \\ \dfrac{d\lambda_i}{ds}\displaystyle\int_\Omega \rho\, u_i \cdot v\, dx - \int_\Omega \frac{d\mathbf{C}}{ds}(s)\epsilon(u_i) \cdot \epsilon(v)\, dx, \\ \\ \forall v \in V. \end{array}\right. \tag{7}$$

where $< u_i >^{\perp}$ *denotes the orthogonal complement of the eigenspace generated by* u_i*, with respect to the inner product in* L^2_ρ*.*

Proof. In order to simplify the notations, the index i will be omitted. Consider the mappings $s \mapsto \lambda(s)$ and $u \mapsto u(s)$, where $u(s)$ is normalized in L^2_ρ . The differentiability results are presented with detail in (Rousselet, 1990). Since $\lambda(s)$ is an eigenvalue and the associated eigenvector $u(s)$ is in the space V, equality (5) holds with $v = u(s)$:

$$\int_\Omega \mathbf{C}(s)\epsilon(u(s)) \cdot \epsilon(u(s))dx = \lambda(s) \int_\Omega \rho u(s) \cdot u(s)dx = \lambda(s).$$

Thus:

$$\begin{aligned} \frac{d\lambda}{ds}(s) &= \frac{d}{ds}\int_\Omega \mathbf{C}(s)\epsilon(u(s)) \cdot \epsilon(u(s))dx \\ &= \int_\Omega \frac{d}{ds}\Big[\mathbf{C}(s)\epsilon(u(s))\Big] \cdot \epsilon(u(s))\, dx + \int_\Omega \mathbf{C}(s)\epsilon(u(s)) \cdot \frac{d}{ds}\epsilon(u(s))\, dx \\ &= \int_\Omega \frac{d\mathbf{C}}{ds}(s)\epsilon(u(s)) \cdot \epsilon(u(s))\, dx + 2\int_\Omega \mathbf{C}(s)\epsilon(u(s)) \cdot \frac{d}{ds}\epsilon(u(s))\, dx. \end{aligned}$$

Taking $v = \dfrac{du}{ds}(s)$ in (5), we conclude that the second term in the last expression is null:

$$\begin{aligned} \int_\Omega \mathbf{C}(s)\epsilon(u(s)) \cdot \epsilon\Big(\frac{du}{ds}(s)\Big)dx &= \lambda(s)\int_\Omega \rho u(s) \cdot \frac{du}{ds}(s)dx \\ &= \frac{1}{2}\lambda(s)\frac{d}{ds}\int_\Omega \rho\, u(s) \cdot u(s)dx \\ &= \frac{1}{2}\lambda(s)\frac{d}{ds}\|u(s)\|^2_{L^2_\rho} \\ &= 0, \end{aligned}$$

Therefore,

$$\frac{d\lambda}{ds}(s) = \int_\Omega \frac{d\mathbf{C}}{ds}(s)\epsilon(u(s)) \cdot \epsilon(u(s))dx.$$

On the other hand, from (5), by derivation with respect to the parameter s it turns out that $\dfrac{du}{ds}(s)$ verifies the following problem:

$$\begin{cases} \displaystyle\int_\Omega \mathbf{C}(s)\epsilon(\frac{du}{ds}(s)) \cdot \epsilon(v)\, dx - \lambda(s) \int_\Omega \rho \frac{du}{ds}(s) \cdot v\, dx = \\ \qquad \displaystyle\frac{d\lambda}{ds}(s) \int_\Omega \rho\, u(s) \cdot v\, dx - \int_\Omega \frac{d\mathbf{C}}{ds}(s)\epsilon(u(s)) \cdot \epsilon(v)\, dx, \\ \qquad\qquad\qquad\qquad\qquad\qquad\qquad\qquad \forall v \in V. \end{cases}$$

According to Fredholm alternative, the above problem has a unique solution if the compatibility condition below holds:

$$\frac{d\lambda}{ds}(s) \int_\Omega \rho\, u(s) \cdot u(s)\, dx - \int_\Omega \frac{d\mathbf{C}}{ds}(s)\epsilon(u(s)) \cdot \epsilon(u(s))\, dx = 0. \quad (8)$$

Since the condition (8) is obviously verified, the derivative $\dfrac{du}{ds}(s)$ is the unique solution of the above problem.

REMARK 1. *For a fixed index i, the above mapping $s \mapsto (\lambda_i(s), u_i(s))$ with $\|u_i\|_{L^2_\rho} = 1$, is not well defined (there are two possibilities, u_i and $-u_i$). However, for the calculation of $\dfrac{du_i}{ds}(s)$ the sign of the eigenvector is important. For this reason, an extra condition is used in the Algorithm proposed in Section 5 to choose the normalized eigenvector: $\displaystyle\int_\Omega u_i(s) \cdot \tilde{u}_i\, dx > 0$. Conversely, for the calculation of $\dfrac{d\lambda_i}{ds}(s)$ this ambiguity doesn't cause any problem.*

REMARK 2. *Since the natural frequency ω_i writes in terms of the eigenvalues λ_i as $\omega_i = \dfrac{\sqrt{\lambda_i}}{2\pi}$, the derivative of ω_i has consequently the form*

$$\frac{d\omega_i}{ds} = \frac{1}{4\pi\sqrt{\lambda_i}} \frac{d\lambda_i}{ds} = \frac{1}{4\pi\sqrt{\lambda_i}} \int_\Omega \frac{d\mathbf{C}}{ds}\epsilon(u_i) \cdot \epsilon(u_i)\, dx. \quad (9)$$

REMARK 3. *The case when the eigenvalues are multiple is an open problem and a subject of future work.*

3. The derivatives of the objective functionals

A straight computation gives the derivative of the functional J_1 defined in (1) as

$$\frac{dJ_1}{ds}(s) = \alpha \sum_{i=1}^{n} \frac{|\,\omega_i(s) - \tilde{\omega}_i\,|^{\alpha}}{\omega_i(s) - \tilde{\omega}_i} \frac{d\omega_i}{ds}(s).$$

and from (9) it turns out that

$$\frac{dJ_1}{ds}(s) = \frac{\alpha}{4\pi} \sum_{i=1}^{n} \frac{|\,\omega_i(s) - \tilde{\omega}_i\,|^{\alpha}}{\omega_i(s) - \tilde{\omega}_i} \frac{1}{\sqrt{\lambda_i(s)}} \int_{\Omega} \frac{d\mathbf{C}}{ds} \epsilon(u_i) \cdot \epsilon(u_i)\, dx. \quad (10)$$

The derivative of J_2 with respect to the parameter s involves the derivatives of the eigenvectors:

$$\frac{dJ_2}{ds}(s) = \frac{dJ_1}{ds}(s) + \sum_{i=1}^{n} c_i \int_{\Omega} \rho \frac{du_i}{ds}(s) \cdot (u_i(s) - \tilde{u}_i)\, dx, \quad (11)$$

where for $1 \leq i \leq n$, c_i are constants equal to $c_i = \alpha \|u_i(s) - \tilde{u}_i\|_{L^2_\rho}^{\alpha-2}$. In order to turn explicit the last term in the above expression of the derivative of J_2, the adjoint method will be employed. Consider n adjoint problems with the form below for $1 \leq i \leq n$:

$$\left\{ \begin{array}{l} \text{find } p_i \in V, \text{ with } \displaystyle\int_{\Omega} \rho p_i \cdot u_i(s) dx = 0 \text{ such that} \\ \displaystyle\int_{\Omega} \mathbf{C}(s)\epsilon(p_i) \cdot \epsilon(w) dx - \lambda_i(s) \int_{\Omega} \rho p_i \cdot w dx = \\ \displaystyle -c_i \int_{\Omega} \rho w \cdot \tilde{u}_i dx + c_i \int_{\Omega} \rho u_i(s) \cdot \tilde{u}_i dx \int_{\Omega} \rho w \cdot u_i(s) dx, \\ \qquad\qquad \forall w \in V. \end{array} \right. \quad (12)$$

Each one of the adjoint problems (12) will allow, by considering a particular test function $w = \dfrac{du_i}{ds}(s)$, to express the terms $c_i \displaystyle\int_{\Omega} \rho \frac{du_i}{ds}(s) \cdot (u_i(s) - \tilde{u}_i)\, dx$. Since $\dfrac{du_i}{ds}(s) \in < u_i(s) >^{\perp}$ the following equality holds

$$c_i \int_{\Omega} \rho \frac{du_i}{ds}(s) \cdot (u_i(s) - \tilde{u}_i) dx = -c_i \int_{\Omega} \rho \frac{du_i}{ds}(s) \cdot \tilde{u}_i dx + c_i \int_{\Omega} \rho u_i(s) \cdot \tilde{u}_i dx \int_{\Omega} \rho \frac{du_i}{ds}(s) \cdot u_i(s) dx,$$

and from the adjoint problem (12), having in mind that $w = \frac{du_i}{ds}(s)$, it turns out that

$$c_i \int_\Omega \rho \frac{du_i}{ds}(s) \cdot (u_i(s) - \tilde{u}_i) dx = \int_\Omega \mathbf{C}(s)\epsilon(p_i) \cdot \epsilon(\frac{du_i}{ds}(s)) dx - \lambda_i(s) \int_\Omega \rho p_i \cdot \frac{du_i}{ds}(s) dx.$$

Using problem (7) that defines $\frac{du_i}{ds}(s)$ with the test function equal to the corresponding adjoint state $v = p_i$, the above term $c_i \int_\Omega \rho \frac{du_i}{ds}(s) \cdot (u_i(s) - \tilde{u}_i) dx$ becomes:

$$\begin{aligned} c_i \int_\Omega & \quad \rho \frac{du_i}{ds}(s) \cdot (u_i(s) - \tilde{u}_i) dx = \\ = \frac{d\lambda_i}{ds}(s) & \int_\Omega \rho u_i(s) \cdot p_i \, dx - \int_\Omega \frac{d\mathbf{C}}{ds}(s)\epsilon(u_i(s)) \cdot \epsilon(p_i) \, dx = \\ = - \int_\Omega & \quad \frac{d\mathbf{C}}{ds}(s)\epsilon(u_i(s)) \cdot \epsilon(p_i) \, dx, \end{aligned}$$

where the last equality holds since p_i belongs to $< u_i(s) >^\perp$. Consequently the derivative of the functional J_2 is obtained in the following explicit form:

$$\begin{aligned} \frac{dJ_2}{ds}(s) = \frac{\alpha}{4\pi} \sum_{i=1}^{n} \frac{|\, \omega_i(s) - \tilde{\omega}_i \,|^\alpha}{\omega_i(s) - \tilde{\omega}_i} \frac{1}{\sqrt{\lambda_i(s)}} \int_\Omega \frac{d\mathbf{C}}{ds}(s)\epsilon(u_i(s)) \cdot \epsilon(u_i(s)) \, dx \\ - \sum_{i=1}^{n} \int_\Omega \frac{d\mathbf{C}}{ds}(s)\epsilon(u_i(s)) \cdot \epsilon(p_i) \, dx, \end{aligned} \tag{13}$$

where p_i, for each $1 \leq i \leq n$, is the solution of the adjoint problem (12) and $(\lambda_i(s), u_i(s))$ is the solution of the variational eigenvalue problem (5).

Note that the last term in (11) could be discretized directly if the functional in consideration has few material parameters subject to optimization. However, this is not feasible for functionals with a large number of parameters as it involves solving $n \times m$ problems given in (11) (where n is the number of modal parameters and m is the number of material parameters). The adjoint method allows for the computation of the derivative of J_2 without the computation of $\frac{du_i}{ds}$ for each material parameter s. Instead, only n adjoint problems (12) are solved.

4. Transversely isotropic constitutive law

The application of the above theoretical results will be done for a concrete dam exhibiting a large zone with cracks in its central part (see Figure 1). This is the case of Cabril dam, located on Zêzere river, in Portugal. Since the cracks are oriented mainly in the horizontal direction, they will be modeled considering a subdomain with transversely isotropic material having smaller elasticity modulus in the vertical direction. The elasticity tensor $\mathbf{C}$ will depend on the material parameters E_z, ν_{zp} and G_{zp} introduced below: $\mathbf{C} = \mathbf{C}(E_z, \nu_{zp}, G_{zp})$.

A transversely isotropic material is characterized by the property of rotational symmetry with respect to one axis. For any direction in the plane orthogonal to this axis (designated "plane of isotropy") the material properties are the same. There are two material parameters which characterize the behavior of the material in this plane: E_p and ν_p. For directions in the axis of symmetry the material properties are different, being described by three other parameters: E_z, ν_{zp} and G_{zp}. The constitutive law for a transversely isotropic material is thus given by five independent material parameters. The strain-stress relation is as follows:

$$\begin{bmatrix} \epsilon_{11} \\ \epsilon_{22} \\ \epsilon_{33} \\ \gamma_{12} \\ \gamma_{23} \\ \gamma_{31} \end{bmatrix} = \begin{bmatrix} \frac{1}{E_p} & \frac{-\nu_p}{E_p} & \frac{-\nu_{zp}}{E_z} & 0 & 0 & 0 \\ \frac{-\nu_p}{E_p} & \frac{1}{E_p} & \frac{-\nu_{zp}}{E_z} & 0 & 0 & 0 \\ \frac{-\nu_{zp}}{E_z} & \frac{-\nu_{zp}}{E_z} & \frac{1}{E_z} & 0 & 0 & 0 \\ 0 & 0 & 0 & \frac{2(1+\nu_p)}{E_p} & 0 & 0 \\ 0 & 0 & 0 & 0 & \frac{1}{G_{zp}} & 0 \\ 0 & 0 & 0 & 0 & 0 & \frac{1}{G_{zp}} \end{bmatrix} \begin{bmatrix} \sigma_{11} \\ \sigma_{22} \\ \sigma_{33} \\ \sigma_{12} \\ \sigma_{23} \\ \sigma_{31} \end{bmatrix}, \tag{14}$$

where γ_{ij} denotes $2\epsilon_{ij}$, that is the engineering strain. The plane of isotropy is assumed to be the $x_1 - x_2$ plane at every point of the subdomain with transversely isotropic material.

5. Description of the numerical algorithm

The whole simulation is implemented in C++ using libMesh open-source framework (Kirk, 2006). The optimization process is accomplished with a line-search procedure using a quasi-Newton method. The implementation is sketched in the Algorithm below. The eigenpairs $(\omega_i, u_i)_{1 \le i \le n}$ in step 1 of the Algorithm are the solutions of the eigenvalue problem (5) with $\mathbf{C} = \mathbf{C}(E_z^{(k)}, \nu_{zp}^{(k)}, G_{zp}^{(k)})$ (the material parameters in iteration k). This eigenvalue problem is solved using Lanc-

Algorithm

Input: the first n measured natural frequencies and corresponding modes, $(\tilde{\omega}_1, \tilde{u}_1), \ldots, (\tilde{\omega}_n, \tilde{u}_n)$; initial guess for the material parameters subject to optimization, $(E_z^{(0)}, \nu_{zp}^{(0)}, G_{zp}^{(0)})$;
Output: values for the material parameters E_z, ν_{zp}, G_{zp} such that the functional is minimized;

for $k = 0, 1, 2, \ldots$ **do**
1. obtain $(\omega_i, u_i)_{1 \leq i \leq n}$ through the resolution of the discretization of the eigenvalue problem (5);
   for $i = 1, \ldots, n$ **do**
2.1. compute the derivatives of the natural frequency ω_i;
2.2. compute the adjoint state p_i as solution of problem (12);
   end for
3. compute J and ∇J;
4. compute a descent direction $d^{(k)}$ using BFGS method;
5. compute an acceptable step length $\alpha^{(k)}$ in order to ensure that the functional J decreases (Wolfe conditions);
6. update the material parameters, $(E_z^{(k+1)}, \nu_{zp}^{(k+1)}, G_{zp}^{(k+1)}) \leftarrow (E_z^{(k)}, \nu_{zp}^{(k)}, G_{zp}^{(k)}) + \alpha^{(k)}\, d^{(k)}$;
7. check convergence;
end for

zos method for eigenproblems. We use the implementation available in the SLEPc open-source library (Hernandez, 2005). The discretization of this problem is done using a mesh with 1456 20-node hexahedral elements (25527 degrees of freedom), shown in Figure 1. Similarly, the computations of J and ∇J in step 3 are relative to the material parameters in iteration k, and use the calculations done in steps 1, 2.1 and 2.2. The descent direction in step 4 is calculated using a quasi-Newton method, namely the BFGS update formula. This computation requires the gradient of J, obtained in step 3. The step length $\alpha^{(k)}$ in step 5 is obtained through a line-search procedure ensuring that the Wolfe conditions are verified (see, for instance, (Dennis, 1996)).

The computation of the adjoint states in step 2.2 is the heavy task of the algorithm. For each $i = 1, \ldots, n$, the adjoint state p_i is the solution of the variational problem (12). The discretization of this problem is a system of linear equations whose matrix has the form $B_i = K - \lambda_i M$, where K and M are the matrices previously obtained in the discretization of the generalized eigenvalue problem in the current iteration (step 1). Thus, B_i is clearly singular and has rank $N - 1$ (where N is the number of degrees of freedom in the simulation). In

this case the hypotheses of the classical Gauss-Seidel method are not fulfilled and it actually diverges. This difficulty can be circumvented by considering a decomposition of the space $\mathbb{R}^N$ as a direct sum of the form $< Mu_1 > \oplus < Mu_2 > \oplus \ldots \oplus < Mu_{i-1} > \oplus < u_1, u_2, \ldots, u_{i-1} >^{\perp}$ (where $\{u_j\}_{1 \leq j \leq i-1}$ is the set of the first $i-1$ eigenvectors obtained in step 1). This decomposition leads to a new system of equations of the form $B_i y = c$, where the right hand side c is different from the one obtained from the discretization of problem (12). The solution y of the new system belongs to $< u_1, u_2, \ldots, u_{i-1} >^{\perp_M}$ (the orthogonal complement for the inner product given by the positive-definite matrix M) and in this framework it is possible to successfully apply a modified version of the Gauss-Seidel method, similar to the one proposed in Chapter 5 of (Barbarosie, 2002). The solution of the adjoint problem p_i is then obtained as a linear combination of the form

$$p_i = y + \sum_{j=1}^{i-1} \beta_j u_j. \tag{15}$$

Since the numerical results will focus on academic examples only, the "measured" natural frequencies and modes of vibration $(\tilde{\omega}_i, \tilde{u}_i)$ will be numerically generated imposing small perturbations to the natural frequencies and modes of vibration $(\bar{\omega}_i, \bar{u}_i)$ that are computed for some prescribed values of the material parameters $(\bar{E}_z, \bar{\nu}_{zp}, \bar{G}_{zp})$. Using this approach, the "exact" modal parameters $(\bar{\omega}_1, \bar{u}_1), \ldots, (\bar{\omega}_n, \bar{u}_n)$ are first computed (before the optimization process begins), by solving the eigenvalue problem (5) with the tensor $\mathbf{C}$ defined by the prescribed material parameters (that is, $\mathbf{C} = \mathbf{C}(\bar{E}_z, \bar{\nu}_{zp}, \bar{G}_{zp})$). Then we define the "measured" natural frequencies $\tilde{\omega}_1, \ldots, \tilde{\omega}_n$ considering a slight perturbation of the "exact" frequencies, $\tilde{\omega}_i = (1 - \xi_i)\bar{\omega}_i$, imposing a perturbation for each frequency equal to ξ_i (ξ_i is a small value). In the same way, the "measured" modes of vibration $\tilde{u}_i$ will be defined as perturbations of the "exact" normalized modes $\bar{u}_1, \ldots, \bar{u}_n$ in the following way:

$$\tilde{u}_i = \bar{u}_i + \sum_{j \neq i} \eta_j \, \bar{u}_j,$$

with η_j small and such that the error $\|\tilde{u}_i - \bar{u}_i\|_{L^2_\rho}$ lays within the same interval of error as the one of $\tilde{\omega}_i$. The functional is defined using these "measured" (perturbed) frequencies and modes $(\tilde{\omega}_i, \tilde{u}_i)_{1 \leq i \leq n}$, and its minimization should give an approximation $(\tilde{E}_z, \tilde{\nu}_{zp}, \tilde{G}_{zp})$ of the parameters $(\bar{E}_z, \bar{\nu}_{zp}, \bar{G}_{zp})$. This procedure is sketched in the following diagram:

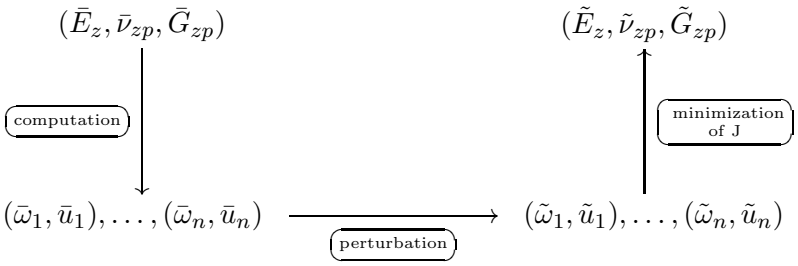

6. Numerical examples

As stated before, the presence of the cracks will be modeled approximately by considering a transversely isotropic material in the subdomain Ω_D, shown in red in Figure 1. In the rest of the dam, $\Omega_I = \Omega \backslash \Omega_D$, an isotropic material will be used since the concrete shows no evidence of cracks or other problems in that part of the body. This way, we consider the body Ω partitioned in two subdomains: an "intact" (isotropic) subdomain Ω_I, and a "damaged" (transversely isotropic) subdomain Ω_D. The material parameters in the isotropic subdomain Ω_I (E and ν) are assumed to be known, so they are fixed in this subdomain. The objective is to find the target material parameters relative to the transversely isotropic material in the subdomain Ω_D. For this reason, the integrals in the formulas from Sections 2 and 3 can be calculated only in Ω_D.

We consider a further simplification by assuming that two of the five parameters of the transversely isotropic material are also known: E_p and ν_p. These parameters are also fixed and set equal to the corresponding parameters in Ω_I. Thus, the remaining parameters to be found through the optimization procedure are E_z, ν_{zp} and G_{zp}. These three parameters characterize the properties of the material in the vertical direction. The list of material parameters treated in the simulations are summarized in Table I. The parameter E_z is related to the parameter E through the damage variable d: $E_z = (1 - d)E$ with $1 < d < 0$.

As for the definition of the funcionals (see (1) and (2)), the power α is set equal to $\alpha = 2$ and the first four natural frequencies and modes of vibration are considered ($n = 4$). The density of the material is $\rho = 2400$ kg/m^3 (same value in both subdomains).

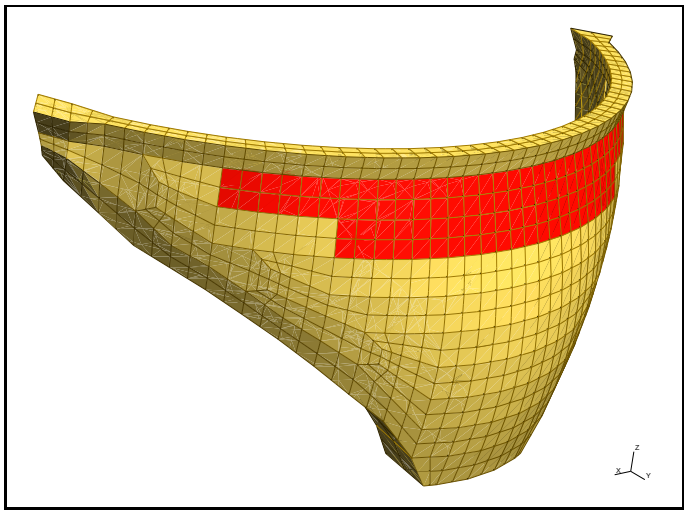

Figure 1. Mesh used in the numerical examples (the elements in red constitute the damaged subdomain).

Table I. List of material parameters considered in the simulations (the subdomain Ω_I has isotropic material, the subdomain Ω_D has transversely isotropic material).

	Fixed parameters	**Variable parameters** (subject to optimization)
$\mathbf{\Omega_I}$	$E^I = 30,\ \nu^I = 0.2$	—
$\mathbf{\Omega_D}$	$E_p^D = 30,\ \nu_p^D = 0.2$	$E_z^D,\ \nu_{zp}^D,\ G_{zp}^D$

6.1. Numerical example 1 - minimization of the functional J_1 (without perturbation)

The first numerical example consists in minimizing J_1 with no perturbation in the "measured" frequencies and modes (that is, $\tilde{\omega}_i = \bar{\omega}_i$, $\tilde{u}_i = \bar{u}_i$). The values of the "exact" natural frequencies $\bar{\omega}_i$ considered are shown in Table III. In this idealized setting, the target (prescribed) values of the three parameters subject to optimization are recovered after 35 iterations of the minimization algorithm. The prescribed target values (used for the calculation of $(\bar{\omega}_i, \bar{u}_i)_{1\leq i\leq 4}$) are arranged in Table II. For the parameter E_z^D, the target value is assigned in terms of a damage variable d as $\bar{E}_z^D = (1-d)\bar{E}^I$, with $d = 0.8$. The initial guess considered is shown in Table IV and corresponds to an isotropic material with the same values as the corresponding parameters in the

Table II. Prescribed values for the material parameters used for the calculation of $(\bar{\omega}_i, \bar{u}_i)_{1\leq i\leq 4}$ in the simulations, see the values of $\bar{\omega}_i$ in Table III.

	Prescribed values
$\mathbf{\Omega_I}$	$\bar{E}^I = 30$ GPa, $\bar{\nu}^I = 0.2$
$\mathbf{\Omega_D}$	$\bar{E}_p^D = 30$ GPa, $\bar{\nu}_p^D = 0.2$, $\bar{E}_z^D = 6$ GPa, $\bar{\nu}_{zp}^D = 0.15$, $\bar{G}_{zp}^D = 2.5$ GPa

Table III. Example 1: first four "exact" natural frequencies $\bar{\omega}_i$, obtained with the prescribed values in Table II (used as "measured" frequencies in the functionals of Examples 1 and 2).

"Exact" frequencies (Hz)
$\tilde{\omega}_1 = \bar{\omega}_1 = 2.52$
$\tilde{\omega}_2 = \bar{\omega}_2 = 2.64$
$\tilde{\omega}_3 = \bar{\omega}_3 = 3.75$
$\tilde{\omega}_4 = \bar{\omega}_4 = 3.81$

isotropic subdomain Ω_I (intact material), that is, the initial guess has the damage parameter equal to zero ($d = 0$).

The history of convergence for J_1 and for the material parameters is displayed in Figure 2. The values reached in the final iteration are shown in brackets and also in Table IV. Note that in the minimization algorithm, the values each parameter is allowed to take is constrained to some reasonable interval. This can be clearly seen in the convergence of ν_{zp}^D. This parameter was constrained to $[0.001, 0.499]$, and the limits of the interval were attained during part of the optimization process.

6.2. Numerical example 2 - minimization of the functional J_2 (without perturbation)

For the second example we consider the functional J_2, again with no perturbation in the "measured" frequencies and modes of vibration. The target values are the same as those used in the previous example (the value of the damage variable is the same), so the frequencies and modes used in the definition of the functional are also the same.

Table IV. Example 1: initial guess for the parameters subject to optimization and corresponding attained values.

Initial guess	Attained values
$E_z^{D(0)} = \bar{E}^I = 30$	$E^D_{z\,\text{final}} = 6.00$
$\nu_{zp}^{D(0)} = \bar{\nu}^I = 0.2$	$\nu^D_{zp\,\text{final}} = 0.15$
$G_{zp}^{D(0)} = \dfrac{\bar{E}^I}{2(1+\bar{\nu}^I)} = 12.5$	$G^D_{zp\,\text{final}} = 2.50$

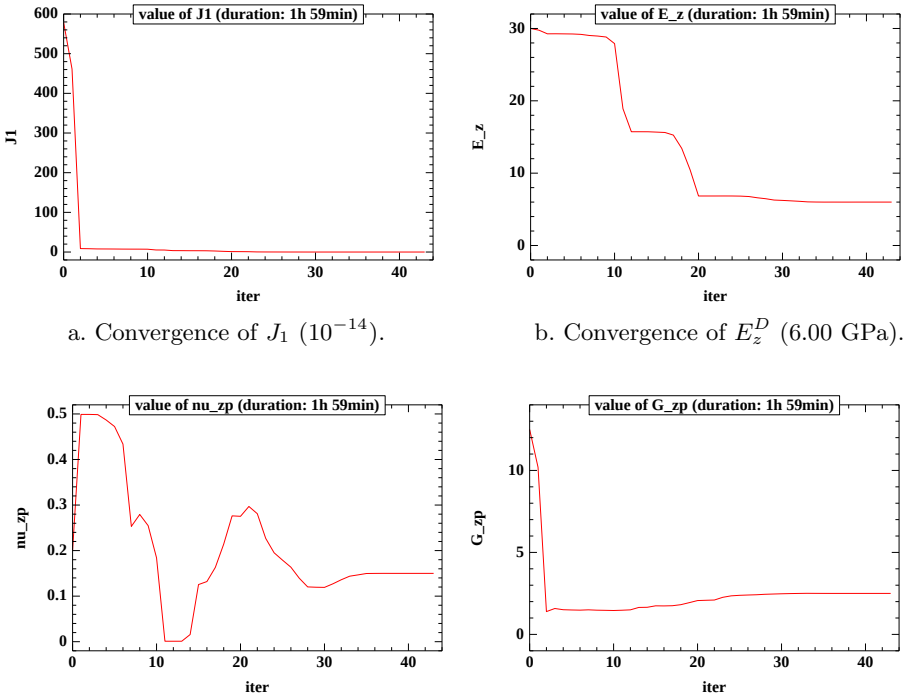

a. Convergence of J_1 (10^{-14}).

b. Convergence of E_z^D (6.00 GPa).

c. Convergence of ν_{zp}^D (0.15).

d. Convergence of G_{zp}^D (2.50 GPa).

Figure 2. Example 1: history of convergence. In brackets are the values reached in the final iteration.

Likewise, the initial guess is the same as in the previous example. The purpose of these choices for the input data is to be able to compare the performance of the two functionals. The configuration taken by the first four modes of vibration $\bar{u}_i$ is shown in Figure 3, with the corresponding frequencies $\bar{\omega}_i$ indicated in the caption. Note that these modes are also used implicitly in the minimization of J_1, as the calculation of $\dfrac{d\omega_i}{ds}$

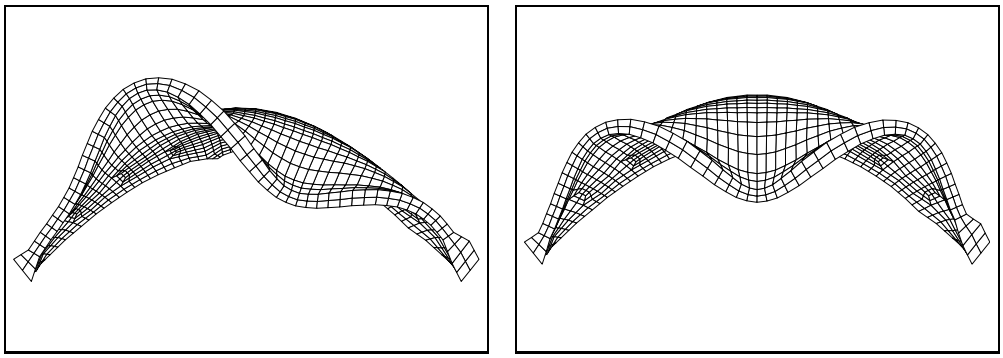

a. First mode (2.52 Hz). b. Second mode (2.64 Hz).

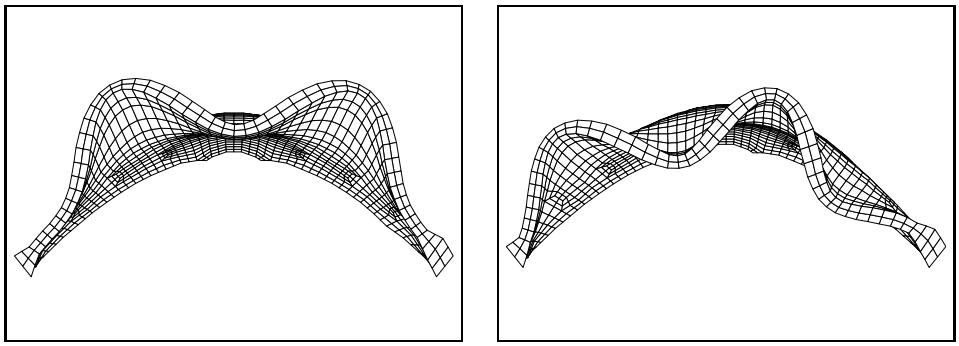

c. Third mode (3.75 Hz). d. Fourth mode (3.81 Hz).

Figure 3. Example 2: first four modes of vibration $\bar{u}_i$ and corresponding natural frequencies $\bar{\omega}_i$ (used in the definition of J_2).

requires $\bar{u}_i$ (see Section 2, formulae (9) and (10)). The history of convergence for this example is displayed in Figure 4, with the attained values shown in brackets. As in the previous example, the target values for the three parameters subject to optimization are recovered. However, with the functional J_2 only 15 iterations were needed until all the three parameters successfully converged to the prescribed target values. The introduction of the modes of vibration works as a kind of constraint, because a mathematical model may have the first natural frequencies close to the measured frequencies and nevertheless present associated modes different from the measured modes.

For this example the definition of the functional is slightly different from the expression given in (2) (see (16) below). Since the derivatives of the term $\sum_{i=1}^{4} \|u_i(s) - \tilde{u}_i\|^2_{L^2_\rho}$ are much smaller than the derivatives of the term $\sum_{i=1}^{4} |\omega_i(s) - \tilde{\omega}_i|^2$, the benefit gained in the minimization algorithm with the introduction of modes of vibration is negligible. To correct this problem two extra coefficients β_1, β_2 are introduced to

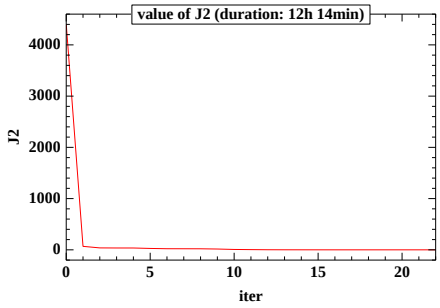

a. Convergence of J_2 (6.27×10^{-10}).

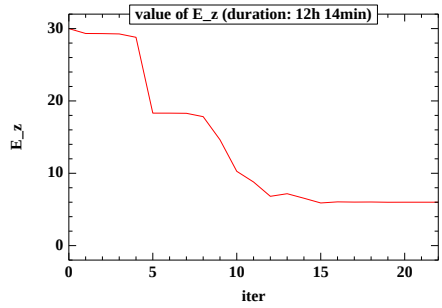

b. Convergence of E_z^D (6.00 GPa).

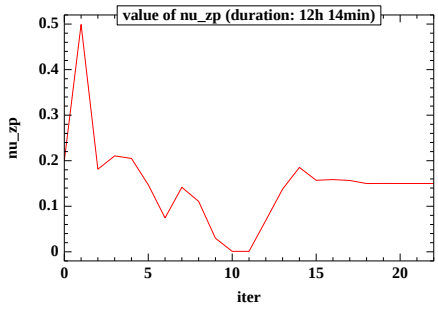

c. Convergence of ν_{zp}^D (0.15).

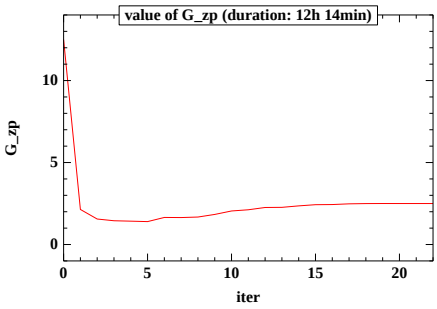

d. Convergence of G_{zp}^D (2.50 GPa).

Figure 4. Example 2: history of convergence. In brackets are the values reached in the final iteration.

adjust the weight of each term in the functional J_2:

$$J_2(E_z, \nu_{zp}, G_{zp}) = \beta_1 \sum_{i=1}^{4} |\omega_i(E_z, \nu_{zp}, G_{zp}) - \tilde{\omega}_i|^2 + \beta_2 \sum_{i=1}^{4} \|u_i(E_z, \nu_{zp}, G_{zp}) - \tilde{u}_i\|_{L^2_\rho}^2. \tag{16}$$

The used values were $\beta_1 = 10^{-3}$ and $\beta_2 = 10^2$.

6.3. Numerical example 3 - minimization of the functional J_2 (with perturbation)

In the third example we use again the functional J_2, this time considering as "measured" frequencies $\tilde{\omega}_i$ and modes $\tilde{u}_i$ a perturbation of the "exact" frequencies $\bar{\omega}_i$ and modes $\bar{u}_i$ (which are obtained with the prescribed target values). As described in Section 5, this perturbation is accomplished in such a way that a specified relative error (which is also prescribed, although in an arbitrary manner) is satisfied. The

Table V. Example 3: first four "exact" frequencies $\bar{\omega}_i$ and perturbed frequencies $\tilde{\omega}_i$ (used as "measured" frequencies in the functional).

i	$\bar{\omega}_\mathbf{i}$ (Hz)	$\tilde{\omega}_\mathbf{i}$ (Hz)	**relative error**
1	2.52	2.38	5.4% (−)
2	2.64	2.51	4.7% (−)
3	3.75	3.61	3.9% (−)
4	3.81	3.64	4.3% (−)

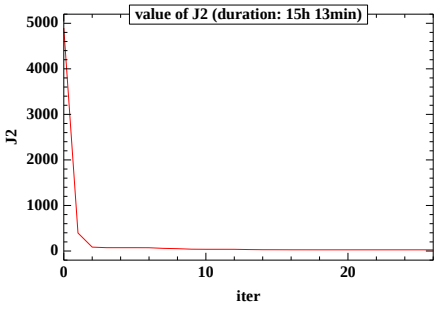

a. Convergence of J_2 (26.03).

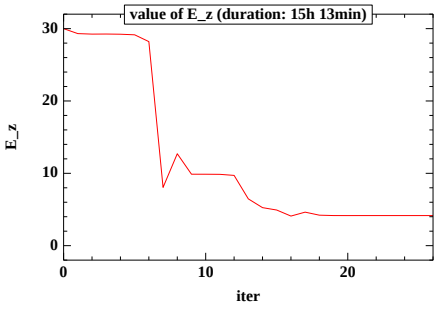

b. Convergence of E_z^D (4.15 GPa).

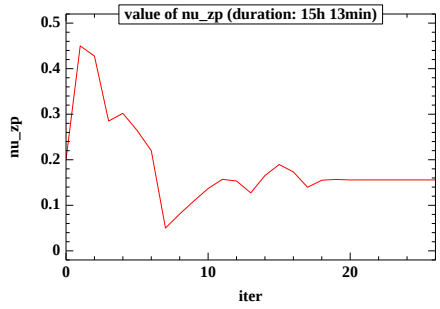

c. Convergence of ν_{zp}^D (0.16).

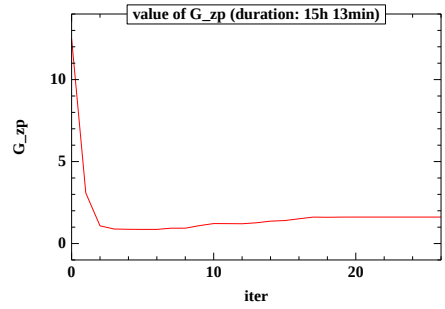

d. Convergence of G_{zp}^D (1.62 GPa).

Figure 5. Example 3: history of convergence. In brackets are the values reached in the final iteration.

values of the perturbed frequencies $\tilde{\omega}_i$ are displayed in Table V. Notice that $\tilde{\omega}_i < \bar{\omega}_i$, $\forall i = 1, \ldots, 4$. In this case, the value to be obtained for E_z^D is expected to be smaller than the prescribed value $\bar{E}_z^D = 6$ (in other words, the attained damage is expected to be greater than the prescribed damage $d = 0.8$). The target values used to obtain the "exact" frequencies $\bar{\omega}_i$ and modes $\bar{u}_i$ are again the values of the previous

examples, shown in Table II. The initial guess is also the same of the previous examples (Table IV).

The history of convergence is displayed in Figure 5. The attained values (in brackets) are relatively close to the target values, but the effect of the perturbations is quite visible in the results. The functional is far from attaining the zero value, as was the case in the previous examples. Nonetheless, the norm of ∇J_2 in the last iterations is of order 10^{-5}. The attained value for the damage variable is $d_{\text{final}} = 0.86$ (higher than the prescribed damage of $d = 0.8$), which was expected taking into account that all the prescribed "measured" frequencies have been reduced (see Table V).

7. Conclusions

We described a method that combines free material design with an inverse optimization problem in order to find the elastic material parameters that fit the measured modal parameters (natural frequencies and modes of vibration) of a dam structure. Academic examples based on the Cabril dam are studied. The main ingredients of the method are the parametric derivatives of the eigenvalues and of the eigenvectors, and the adjoint method. These tools allow the use of gradient type methods to solve the minimization problem. Two functionals are proposed to be minimized: J_1, depending only on the natural frequencies, and J_2, depending on the natural frequencies and on the modes of vibration. We note that the functionals J_1 and J_2 considered are highly non-linear and have several minima. In the case of modal parameters corresponding to some known material parameters, the functional J_2 proved to have a better behavior in the optimization process, needing only half of the iterations required by J_1 to converge (though the total time of the simulation is greater with J_2). The performed numerical optimization tests show that the use of lower "measured" natural frequencies leads to the identification of higher damage values in the deteriorated zone of the dam.

In the future we intend to generalize this method in several ways. The most direct development is to use a different constitutive linear elastic law instead of the transversely isotropic law. We could also allow the material parameters to vary from element to element in the damaged zone, in order to allow for different degrees of damage. Finally, to make the simulation more realistic, the effect of water in the modal parameters should be taken into account using, for example, H.M. Wastergaard's approach (Westergaard, 1933), or water finite elements formulated in displacements or pressures (Hall, 1983), (Severn, 1991).

On a technical level, the C++ code will be improved to allow the parallel computation of the derivatives of the eigenvalues and of the adjoint states, as these calculations are completely independent of each other. This upgrade should significantly reduce the running time of the algorithm.

Acknowledgements
This work was supported by FCT, Financiamento Base 2010, ISFL-1-209.

References

Barbarosie, C. *Análise assimptótica e optimização de microestruturas em mecânica dos meios contínuos*. PhD thesis, Faculdade de Ciências da Universidade de Lisboa, 2002.

Bendsoe, M.P. *Optimization of structural topology, shape and material*. Springer, 1995.

Dautray, R. and J.-L. Lions *Analyse Mathématique et Calcul Numérique pour les Sciences et les Techniques - Tome 2*. Masson, 1985.

Dennis, J. and R. Schnabel *Numerical Methods for Unconstrained Optimization and Nonlinear Equations*. SIAM, 1996.

Comissão Nacional Portuguesa das Grandes Barragens, *Large Dams in Portugal*. Edição CNPGB, 1992. `http://cnpgb.inag.pt/gr_barragens/gbportugal/Cabril.htm`

Hall, J.F and A.K. Chopra Dynamic analysis of arch dams including hydrodynamic effects. *Journal of Engineering Mechanics Division*, ASCE 1983, 109(1):149-163, 1983.

Hernandez, V., J.E. Roman and V. Vidal SLEPc: A Scalable and Flexible Toolkit for the Solution of Eigenvalue Problems. *ACM Transactions on Mathematical Software*, 31(3):351-362, 2005. `http://www.grycap.upv.es/slepc/`

Kirk, B., J.W. Peterson, R.H. Stogner and G.F. Carey libMesh: A C++ Library for Parallel Adaptive Mesh Refinement/Coarsening Simulations. *Engineering with Computers*, 22(3-4):237-254, 2006. `http://libmesh.sourceforge.net/`

Mota Soares, C.M., M. Moreira de Freitas, A.L. Araújo and P. Pedersen Identification of Material Properties of Composite Plate Specimens. *Composite Structures*, 25(1-4):277-285, 1993.

Oliveira, S. Continuous monitoring system for the dynamic performance assessment of arch dams. Sub-programme D. in *Study of evolutive deterioration processes in concrete dams. Safety control over time*. Nat. sci. re-equipment programme of FCT (REEQ/815/ECM/2005).

Oliveira S., P. Mendes, A. Garrett, O. Costa and J. Reis Long-term dynamic monitoring systems for the safety control of large concrete dams. The case of Cabril dam, Portugal. *Proceedings of the 6th International Conference on Dam Engineering*. Lisbon, Portugal, 2011.

Pagnotta, L. Recent Progress in Identification Methods for the Elastic Characterization of Materials. *International Journal of Mechanics*, 2(4):129-140, 2008.

Rousselet, B. and D. Chenais Continuité et Différentiabilité d'Éléments Propres: Application à l'Optimisationde Structures. *Applied Mathematics and Optimization*, 22(1):27-59, 1990.

Severn, R.T. and E.J. Greeves State of the art review of the analysis and modelling of fluid-structure interaction. *Structures Subject to Dynamic Loads*, 233-270, Elsevier 1991.

Westergaard, H.M. Water pressure on dams during earthquakes. *Transactions A.S.C.E.*, 90(1835):418-433, 1933.